Catalysis Science & Technology

Accepted Manuscript

ROYAL SOCIETY OF CHEMISTRY

www.rsc.org/catalysis

Catalysis Science & Technology

Cite this: DOI: 10.1039/c0xx00000x

PAPER

www.rsc.org/xxxxxx

Nanosheets of graphitic carbon nitride as metal-free environmental photocatalysts

Zhijun Huang, Fengbo Li,* Bingfeng Chen, and Guoqing Yuan*

Received (in XXX, XXX) Xth XXXXXXXXX 20XX, Accepted Xth XXXXXXXXX 20XX

DOI: 10.1039/b000000x

Nanosheets of graphitic carbon nitride were prepared through direct heat treatment of guanidinium chloride at 450-600 ℃ in air atmosphere. The resulting materials had a surface area of 109.9 m^2/g and their physicochemical properties were closely related to condensation temperature. Decomposition of rhodamine (RhB) in aqueous solution was selected as the model reaction to investigate the photocatalytic performance of nanostructured graphitic carbon nitride. The sample with higher surface area exhibited better optical properties and had enhanced photocatalytic activity. These findings suggest that graphitic carbon nitride prepared from guanidinium chloride will be promising for use in pollutants degradation and solar energy utilization.

1. Introduction

With the rapid development of modern industry, a large amount of industrial wastewater containing organic pollutants are discharged into the land and water bodies and cause significant harm to the ecological environment. Many methods have been employed for the removal of organic pollutants from wastewater, such as biological treatment and adsorption.[1, 2] But their low efficiency and hazardous byproducts limit their practical applications. Photocatalytic oxidation has become one of the most efficient techniques for the removal of organic pollutants, because of its mild operating condition, low power consumption and strong decontamination ability. During the past four decades, a variety of photocatalysts have been explored, including metal oxides, [3, 4] sulfides,[5] nitrides[6] and phosphides.[7] However, it remains a problem in developing inexpensive, environmentally friendly and efficient photocatalyst.

Graphitic carbon nitride (g-C_3N_4) was reported to produce hydrogen from water under visible-light irradiation [8] and this organic semiconductor photocatalyst had gradually attracted significant attention because of their promising applications in pollutants degradation and solar energy utilization. [9-12] Recent novel findings revealed that conjugated carbon nitride nanostructures were promising catalysts for photoredox and hydrogen photosynthesis. [13-15] G-C_3N_4 was generally synthesized by self-condensation of nitrogen-rich precursors, such as cyanamide, dicyanamide or melamine. However, the resulting g-C_3N_4 solids were bulk materials with poor porous properties. Their BET surface areas (S_{BET}) were below 10 m^2 g^{-1} and this directly led to their low catalytic activty. To solve this problem, well-dispersed g-C_3N_4 nanophases loaded in SBA-15 mesochannels were prepared and their catalytic performances were improved significantly with the increase of S_{BET}.[16, 17] Nanocasting was another commonly used and efficient technique to modify the structure of g-C_3N_4. Colloidal silica spheres or mesoporous silica were successfully used as hard templates to prepare porous g-C_3N_4.[18-21] Surface acidification and sonication-promoted insertion technologies were used to fabricate g-C_3N_4 with ordered 2D mesoporous hexoagonal framework The largest S_{BET} of the as-prepared samples was up to 517 m^2 g^{-1} and they had enhanced photocatalytic activity towards hydrogen evolution.[20] In addition, porous g-C_3N_4 materials were synthesized by soft-templating methods.[22-24] Boron- and fluorine-enriched mesoporous g-C_3N_4 with narrow pore size distribution had been synthesized by using room-temperature ionic liquid as soft-template. The as-prepared materials exhibited improved photoactivity under visible-light illumination.[23] However, the use of synthesis templates was not economic and environmentally friendly. Recently, g-C_3N_4 with S_{BET} of 96.6 m^2 g^{-1} was synthesized from urea, an oxygen-containing precursor without the assistance of any template. Due to the high S_{BET}, the prepared g-C_3N_4 exhibited enhanced photocatalytic activity for RhB degradation and hydrogen production.[25-27] Except for urea, some other unconventional precursors were also used to prepare g-C_3N_4, such as cyanuric acid−melamine complex,[28-30] thiourea, [31, 32] melamine hydrochloride,[33] melamine nitrate,[34] NH_4SCN [35] and trithiocyanuric acid. [36] Owing to the peculiar nanostructures, high surface area, improved optical and electrical properties, most of the as-prepared g-C_3N_4 materiasl exhibited higher catalytic activity than that of the materials synthesized from traditional precursors.

Guanidinium chloride (GndCl), an environmentally benign and widely available precursor, was used for the synthesis of mesoporous g-C_3N_4 under Ar atmosphere via nanocasting method by using colloid silica as the template.[37] However, a hazardous reagent (NH_4HF_2) was used to remove the template. This process was time-consuming and led to heavy pollution. In this work, novel nanostructured g-C_3N_4 was easily prepared through GndCl self-condensation under heat treatment during 450-600 ℃ in air

atmosphere without the assistance of any template. The resultant materials had a microstructure of nano-sheet with a high S_{BET} of 109.9 m^2/g. The photocatalytic performances of the resultant g-C_3N_4 were investigated by rhodamine (RhB) degradation under light irritation, and compared with that of g-C_3N_4 prepared from melamine.

2. Experimental

2.1. Preparation of catalysts

All the reagents were analytical-grade and used as received. Catalysts were prepared by directly condensation of GndCl in still air atmosphere. Typically, 5 g of GndCl was put into a covered crucible, and then heated to a certain temperature in muffle furnace for 4 h with a heating rate of 10 ℃ min^{-1}. The resultant yellow samples were denoted as CN-*x*, where *x* refers to the condensation temperature. For comparison, g-CN was also prepared from melamine at 600 ℃ using the same heating program.

2.2. Characterization and methods

The powder X-ray diffraction (XRD) patterns were measured on Rigaku Rotaflex diffractometer equipped with a rotating anode and a Cu Kα radiation source (40 kV, 200 mA; λ= 1.54056 Å). Fourier transform infrared (FT-IR) spectra were recorded on a Bruker Tensor 27. X-ray photoelectron spectroscopy (XPS) dates were obtained on a Thermo Scientific ESCALab 250Xi using 200 W monochromated Al Kα radiation. The 500 μm X-ray spot was used for XPS analysis. The base pressure in the analysis chamber was about 3×10^{-10} mbar. The hydrocarbon C1s line at 284.8 eV from adventitious carbon is used for energy referencing. Elemental analysis (EA) results were collected from a Flash EA 1112. The nitrogen adsorption and desorption isotherms were determined at 77.3 K by a Quanta-chrome Autosorb Automated Gas Sorption System (Quantachrome Corporation) after samples were dried at 300 ℃ under vacuum for 6 h. The transmission electron microscopy (TEM) images were obtained on a JEOL JSM-2100 instrument with an accelerating voltage of 200 kV. UV-vis diffuse reflectance spectra (DRS) were obtained using a UV-vis spectrometer (Shimadzu UV-2600) equipped with an integrating sphere assembly. $BaSO_4$ was used as reference. Photoluminescence spectra (PL) were recorded with a fluorescence spectrometer (Hitachi F-4500) with excitation at 350 nm at room temperature.

2.3 Photocatalytic actvity test

Degradation of RhB under light irritation was chosen as a model reaction to investigate the photocatalytic activities of the prepared g-C_3N_4. The light was provided by a 500 W xenon lamp with a jacket filled with flowing water to keep the system cool. Typically, 50 mg of catalyst was stirred in 100 ml of RhB aqueous solution (10 mg L^{-1}) in the dark for 1h. When the adsorption-desorption equilibrium was achieved, the light was turned on to start the photocatalytic reaction. At 10 min intervals, about 4 mL of suspension was collected and centrifuged at 12 000 rpm for 10 min to remove the catalysts. The upper clear liquid was analyzed by UV-vis absorption spectra. The maximum absorption was recorded at 553 nm and used for evaluating the concentration of RhB. The degradation rate and rate constant *k* are calculated by equation (1) and (2) respectively as follows:

$$\text{Degradation rate} = (C_0 - C)/C_0 \times 100\% \quad (1)$$

$$\ln(C/C_0) = -kt \quad (2)$$

Where, C_0 is the adsorption-desorption equilibrium concentration of RhB and C is the concentration of RhB at reaction time of t.

3. Results and discussion

3.1 The development of g-C_3N_4 nano-sheets

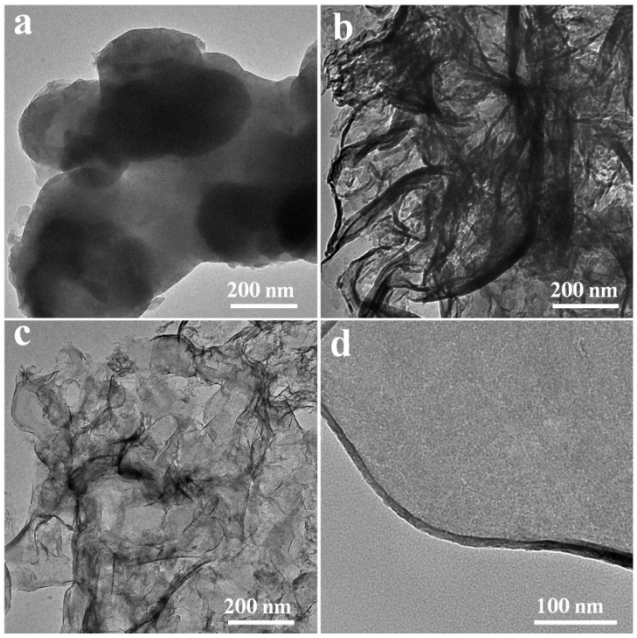

Fig. 1 TEM images of g-CN (a), CN-450 (b) and CN-600 (c) - (d).

The morphological structures of the samples are characterized by TEM measurements. G-C_3N_4 prepared from melamine exhibits agglomeration of large particles (Fig. 1a). Thermal self-condensation of GndCl leads to the development of flaky structures. Fig. 1b shows microstructures of the sample prepared at 450 ℃ and the incipient formtion of sheet-like structures can be revealed. With the increase of treatment temperature, well-dispersed nanosheets of g-C_3N_4 are prepared at 600 ℃ (Fig. 1c). Fig. 1d clearly shows the edge of a single nanosheet of CN-600. Rolling up of the edge may reduce the surface energy of the nanosheet and improve its stability.

The development of nanosheets of g-C_3N_4 under different treatment temperature was characterized by powder XRD. The sample treated at 400 ℃ shows a complicated XRD pattern that indicates the low polymerization degree (Fig. 2a). When the condensation temperature increased to 450 ℃, two characteristic diffraction peaks at 13.3° and 27.3° are detected, which suggest the incipient formation of g-C_3N_4. With the increase of treatment temperatute, the diffraction peaks become sharper and stronger. This indicates more ordered graphitic-like layered structure and higher crystallinity are gradually developed. The increase of treatment temperature gradually causes shift of the typical (002) interlayer-stacking peak from 27.3° to 27.6° (Fig. 2b). This indicates that the interlayer distance of g-C_3N_4 decreases with the increasing condensation temperature.[25]

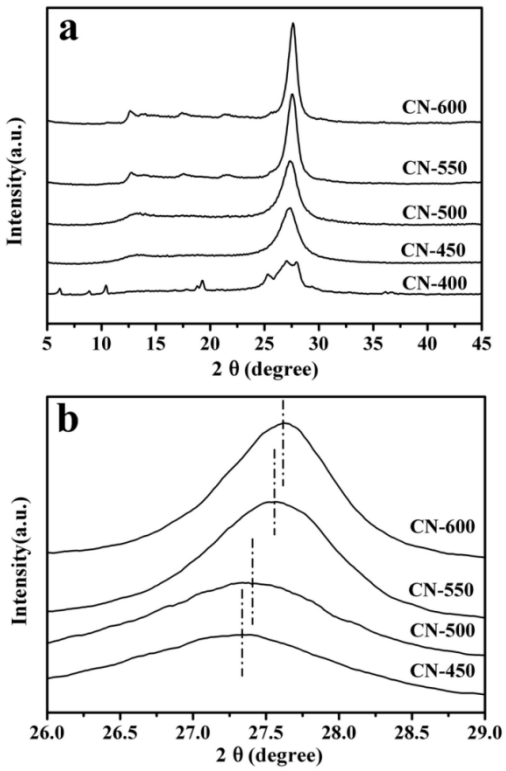

Fig. 2 a) Powder XRD patterns of g-C_3N_4 prepared from self-condesation of GndCl under different treatment temperature. b) Shift of (002) interlayer-stacking peak with the increase of treatment temperature.

The formation of g-C_3N_4 is further confirmed by FT-IR patterns in Fig. 3. The result is similar to that of XRD characterization. FT-IR pattern of CN-400 shows typical stretching modes of C-N heterocycles in the 1200−1650 cm^{-1} region, although it is not remarkable. Additionally, the breathing mode of triazine units at 810 cm^{-1} is also appeared. This indicates the incomplete condensation of GndCl at 400 ℃. When increasing the condensation temperature to 450 ℃, the typical FT-IR pattern of g-C_3N_4 appeare and suggests the formation of g-C_3N_4. With further increase in treatment temperature, the FT-IR bands become stronger and sharper, which is attributed to the higher degree of polymerization.

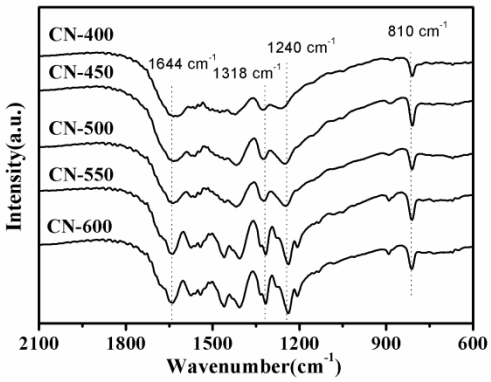

Fig. 3 FT-IR patterns of the g-C_3N_4 prepared from self-condesation of GndCl under different treatment temperature.

3.2 The chemical compositions and porous structures of g-C_3N_4 nanosheets

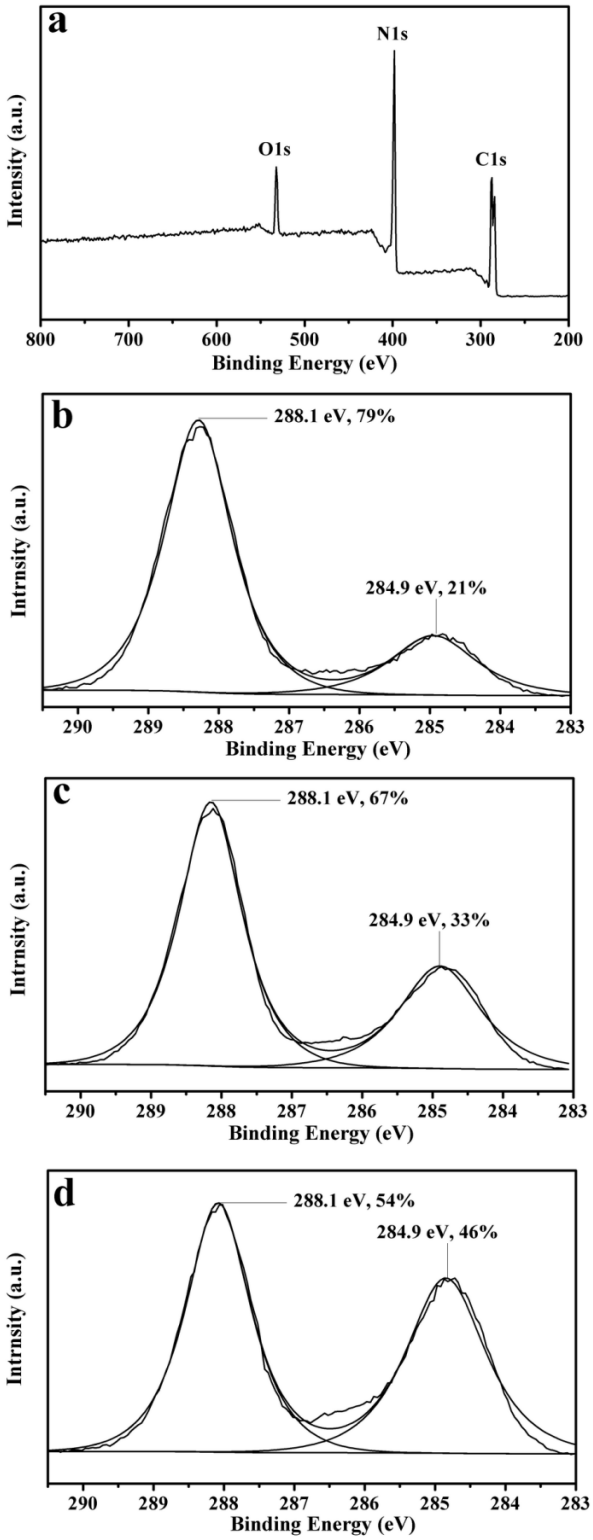

Fig. 4 a) XPS survey spectrum of CN-600. b) C1s XPS peaks of g-C_3N_4 from melamine (g-CN). c) C1s XPS peaks of g-C_3N_4 from self-condesation of GndCl at 450 ℃ (CN-450). d) C1s XPS peaks of g-C_3N_4 from self-condesation of GndCl at 600 ℃ (CN-600).

Fig. 4 shows the XPS spectra of g-CN, CN-450 and CN-600. As shown in XPS survey spectrum of CN-600 (Fig. 4a), the main elements on the surface of are C, N. There is a small amount of oxygen, which is mainly attributed to the adsorbed water and carbon dioxide. The XPS survey spectra of other samples are similar to that of CN-600. Table 1 summarizes the surface and bulk C/N atomic ratio measured by XPS and element analysis respectively. Bulk C/N atomic ratios for all the samples are about 0.67. Chemical compositions of g-C_3N_4 prepared from GndCl are similar to the g-C_3N_4 prepared from melamine. However, the surface C/N atomic ratio of g-CN is 0.92, which is higher than bulk C/N atomic ratio. The higher surface C/N atomic ratio implies a certain amount of surface nitrogen was burned during condensation in air atmosphere.[38] In addition, the surface C/N atomic ratio of CN-450 is increased to 1.07, and further increased to 1.46 for CN-600. This increasing trend indicates that the effect of precursor and condensation temperature on the surface chemical composition of the obtained samples is remarkable. The high-resolution XPS spectra of C1s were selected to further investigate the surface chemical compositions of different samples. As revealed in Fig. 4b, c and d, the XPS spectra of C1s for all the three samples can be fitted into two peaks. The peak at binding energy of 288.1 eV is attributed to tri-*s*-triazine in lattice, and the peak at 284.9 eV is attributed to pure carbon such as graphite or amorphous carbon.[16] No obvious binding energy shift indicates that the chemical states of carbon in CN-*x* are similar to that of g-CN. However, the content of pure carbon for different samples is different. It increased from 21% for g-CN to 33% for CN-450, and further increased to 46% for CN-600, implying that the surface carbon content of CN-*x* is higher than that of g-CN with the trend of the increasing condensation temperature, which is in accordance with the results depicted above.

The S_{BET} of CN-*x* obtained at different temperature are shown in Fig. 5a. The values increase markedly with the increase of condensation temperature. The S_{BET} of CN-450 is 22.9 m^2 g^{-1}, and it increases to 109.9 m^2 g^{-1} for CN-600. It should be note that the S_{BET} of g-CN prepared from melamine at 600 ℃ is 19.8 m^2 g^{-1}, which is much lower than that of CN-600. The high S_{BET} of g-C_3N_4 obtained from GndCl may be mainly due to the release of HCl and NH_3 during condensation.[31, 39] Additionally, thermal oxidation etching in air atmosphere is another reason for the high S_{BET}.[35] Fig. 5b shows the N_2 adsorption and desorption isotherms of g-CN and CN-600. CN-600 possesses a typical type Ⅲ isotherm with H3 hysteresis loop at 0.50 < P/P0 < 1.00, which is attributed to the aggregation of plate-like particles giving rise to slit-shaped pores.[33, 39]

Table 1 C/N atomic ratio of different samples

	g-CN	CN-450	CN-600	CN-600 [a]
Surface	0.92	1.07	1.46	1.64
Bulk	0.67	0.66	0.67	0.67

[a]: after reaction.

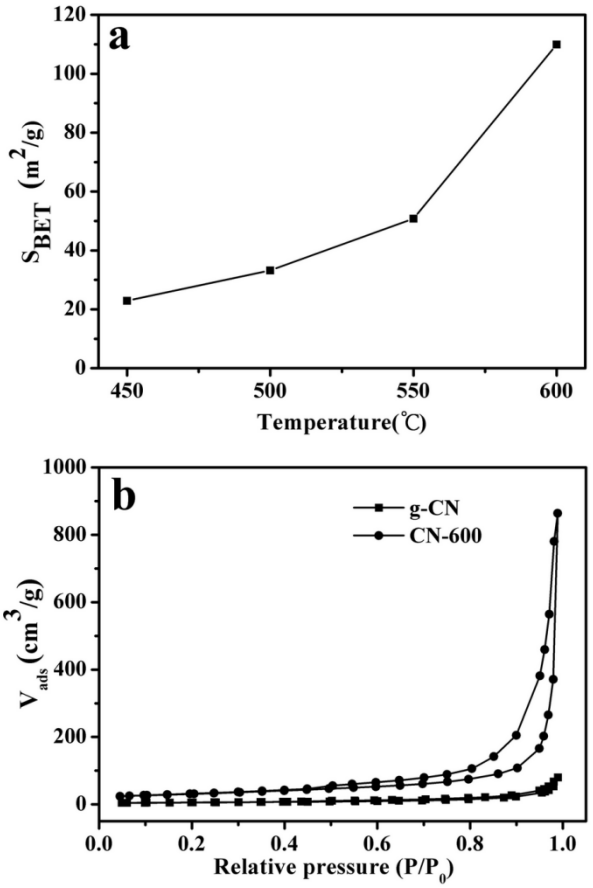

Fig. 5 a)The relationship between S_{BET} and the condensation temperatures. b) N_2 adsorption–desorption isotherms of g-CN and CN-600.

3.3 The optical properties of g-C_3N_4

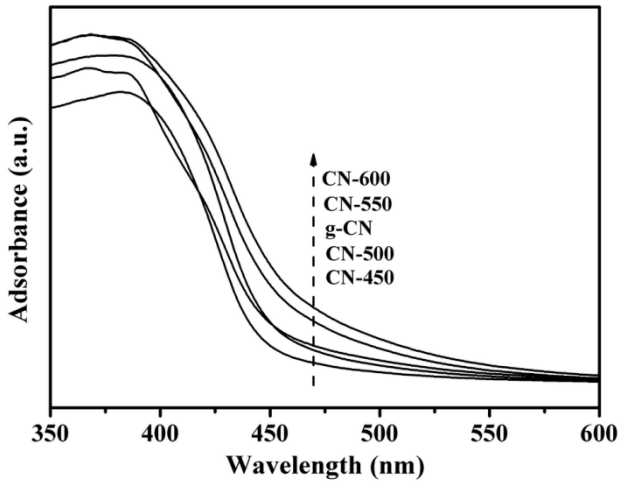

Fig. 6 UV-vis spectra of different g-C_3N_4 samples.

Fig. 6 is the UV-vis spectra of CN-*x* obtained at different condensation temperatures, and compared with the spectrum of g-CN. All samples exhibit strong UV absorption. Due to the quantum confinement effect of the less layer thickness, the absorption edge of CN-450 is blue shifted from 460 nm for g-CN

to 440 nm. [18, 40] As verified by TEM measurements, the layer thickness of CN-*x* is decreased with the increasing condensation temperature. However, the absorption edge of CN-*x* is red-shifted with the trend of increasing condensation temperature in despite of the quantum confinement effect. The absorption edge of CN-600 is 510 nm, which is 50 nm red-shifted compared with that of g-CN. The enhanced optical absorption may be caused by the different surface chemical compositions of the samples. As depicted above, with the increase of condensation temperature, the surface carbon content of CN-*x* is increased gradually. Theoretic computation [41] and experimental investigation [22, 42] revealed that modification of g-C_3N_4 with a small amount of carbon resulted in strong electronic coupling at the interface of the two substances.

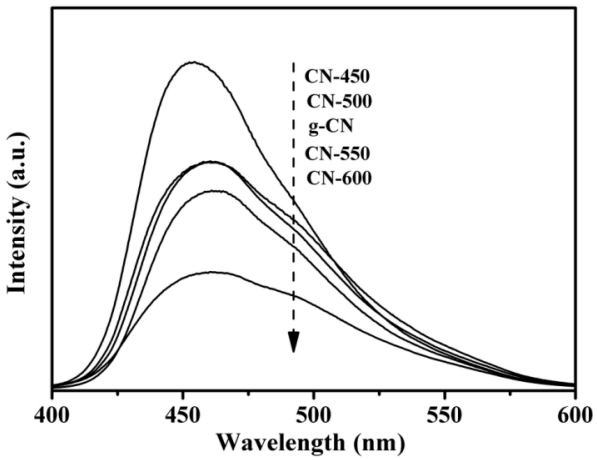

Fig. 7 PL spectra of different g-C_3N_4 samples.

PL spectra are further employed for evaluating the optical and electronic properties of the prepared g-C_3N_4. As shown in Fig. 7, CN-450 exhibits the highest PL intensity. However, the PL intensities decrease gradually with the increasing condensation temperatures because of the quantum confinement effect and the increased surface carbon content.[42, 43] The PL intensity of g-CN is similar to that of CN-500, but is much higher than that of CN-550 and CN-600. The lower PL intensity of CN-550 and CN-600 means the higher efficiency in the migration, transfer and separation of the photogenerated charge carriers, [39, 44] which are beneficial for their photocatalytic performance.

3.4 The photocatalytic activities and stabilities of g-C_3N_4 nanosheets

Degradation of RhB under light irritation is used to evaluate the photocatalytic activities of the catalysts. The light is provided by a 500 W xenon lamp. The amount of RhB adsorbed to the g-C_3N_4 is increased with the increase of S_{BET} and the proportions are all less than 15%. As shown in Fig. 8a, RhB can be degraded over all the tested catalysts under light irradiation, but it is obvious that the photocatalytic activities for all the CN-*x* obtained from GndCl are higher than that of g-CN obtained from melamine. For g-CN, the degradation rate of RhB is 24%. When CN-600 was used as catalyst, the degradation rate is increased to nearly 100%, more than four times higher than that of g-CN. In order to quantitatively investigate the reaction kinetic, the rate constants of the reaction over different catalysts were also calculated and presented in Fig. 8b. It can be seen that the rate constant for g-CN is 0.0046 min^{-1}, and it increased largely to 0.051 min^{-1} for CN-600. The enhanced activity of CN-600 is mainly due to the high S_{BET}. The high S_{BET} could not only provide more catalytic active sites, but also benefit for the adsorption and diffusion of reactants, thus speeding up the reaction rate. For the same reason, the catalytic activity of CN-*x* is increased with the increasing condensation temperature as demonstrated in Fig. 8a and b. In addition to S_{BET}, optical properties of the catalyst also influence its catalytic activity. Compared with g-CN, the optical absorption and charge transfer of CN-*x* have been enhanced with the increase of condensation temperature, which also helpful to improve their photocatalytic performances.

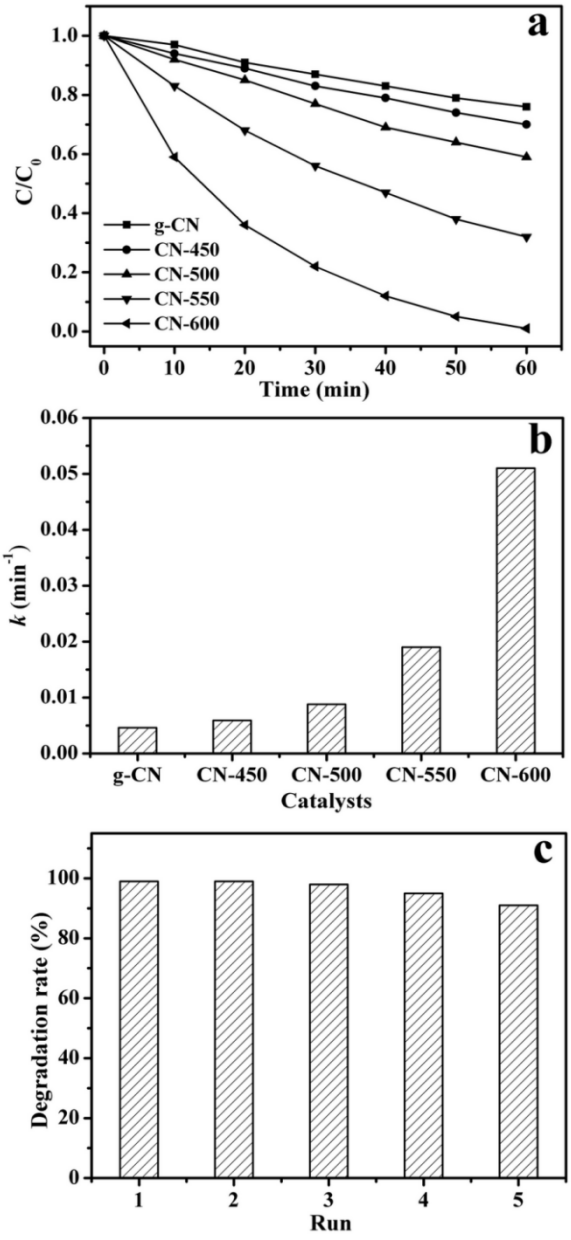

Fig. 8 a) Photocatalytic activities of various g-C_3N_4 samples. b) Calculated rate constants of g-C_3N_4 samples for the degradation of RhB. c) Five-run recycling test of CN-600.

Generally, g-C_3N_4 materials have excellent thermal and chemical stability.[10, 45] To examine the stability of g-C_3N_4 nanosheets from GndCl, the recyclability of the as-prepared catalyst was investigated in a five-run recycling test of catalytic RhB degradation. The test was carried out over CN-600, which exhibits the best photocatalytic performance. As revealed in Fig. 8c, the degradation rate of RhB has not been decreased significantly within five runs. It dropped slightly from 99% for the first run to 91% for the fifth run. This indicates that the catalysts obtained from GndCl have excellent photocatalytic stability.

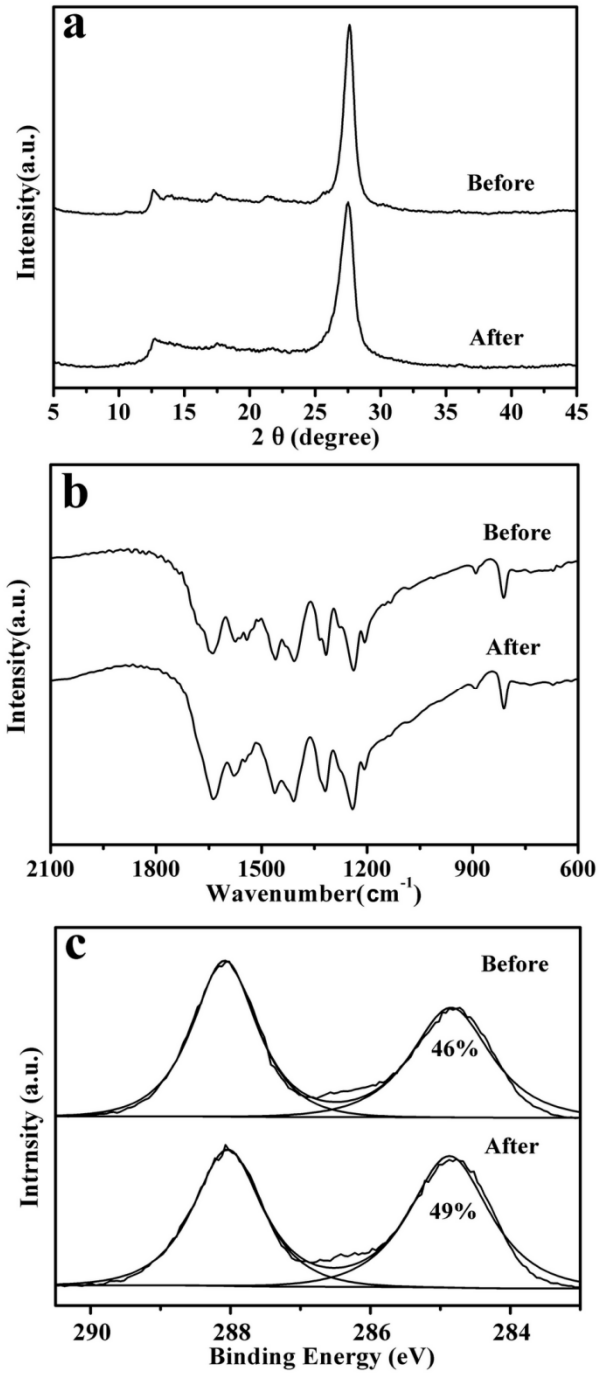

Fig. 9 The XRD (a) FT-IR (b) and XPS (c) patterns of CN-600 before and after the five-run recycling test.

To further investigate the stability of CN-*x*, the used CN-600 was characterized by XRD, FT-IR and XPS spectra, and compared with those of fresh CN-600 catalyst. It is clearly showed in Fig. 9a and b that the XRD and FT-IR patterns of the used CN-600 have not been changed remarkably. This suggests that the crystal and chemical structures of CN-*x* are stable during the reactions. However, the surface C/N atomic ratio of CN-600 is increased slightly from 1.46 to 1.64 after the reaction (Table 1). This is in accordance with the results of Fig. 9c. The content of pure carbon at binding energy of 284.9 eV is increased from 46% to 49%. The increased surface carbon is probably ascribed to the adsorbed RhB and its degradation products, which is responsible for the slightly decreased catalytic activity.

4. Conclusions

In summary, g-C_3N_4 nanosheets have been successfully synthesized from GndCl in air between 450 and 600 ℃. The release of HCl and NH_3 and thermal oxidation etching during condensation give the samples with high S_{BET}. In addition, the condensation temperature has great effect on the properties of the obtained g-C_3N_4. Both crystallinity and S_{BET} increase as the condensation temperature increasing. Furthermore, the surface carbon contents of CN-*x* also increase when elevating condensation temperature, and thus improving their optical properties. The as-prepared g-C_3N_4 nanosheets exhibit much higher catalytic activities for photo-degradation of RhB than that of g-C_3N_4 prepared from melamine. The high S_{BET} and optimized optical properties are contributed to the enhanced photocatalytic activity. Considering the excellent photocatalytic performance, the facile synthesis process and the economic advantages of the precursor, g-C_3N_4 nanosheet from GndCl self-condesation is a promising candidate for pollutants degradation and solar energy utilization.

Acknowledgements

This work was supported by the Natural Science Foundation of China (21304101, 21101161, 21174148) and Beijing YMB New Energy Technology Co., Ltd..

[a] *Beijing National Laboratory of Molecular Science, Laboratory of New Materials, Institute of Chemistry, Chinese Academy of Sciences, Beijing (PR China). Fax: (+86) 10-62559373; E-mail: lifb@iccas.ac.cn, yuangq@iccas.ac.cn*
[b] *University of Chinese Academy of Sciences, Beijing, 100049 (PR China)*

Notes and references

1 H. L. Jiang, J. H. Tay, A. M. Maszenan, S. T. L. Tay, *Environ. Sci. Technol.*, 2006, **40**, 6137.
2 I. Ali, M. Asim, T. A. Khan, *J. Environ. Manage.*, 2012, **113**, 170.
3 K. Maeda, *Chem. Commun.*, 2013, **49**, 8404.
4 A. Fujishima, K. Honda, *Nature*, 1972, **238**, 37.
5 K. Ikeue, Y. Shinmura, M. Machida, *Appl. Catal., B*, 2012, **123-124**, 84.
6 Y. Cong, H. S. Park, H. X. Dang, F.-R. F. Fan, A. J. Bard, C. B. Mullins, *Chem. Mater.*, 2012, **24**, 579.
7 Y. Wang, Y. Wang, R. Jiang, R. Xu, *Ind. Eng. Chem. Res.*, 2012, **51**, 9945-9951.
8 X. Wang, K. Maeda, A. Thomas, K. Takanabe, G. Xin, J. M. Carlsson, K. Domen, M. Antonietti, *Nat. Mater.*, 2009, **8**, 76..

9 A. Thomas, A. Fischer, F. Goettmann, M. Antonietti, J. O. Müller, R. Schlögl, J. M. Carlsson, *J. Mater. Chem.*, 2008, **18**, 4893.

10 Y. Wang, X. Wang, M. Antonietti, *Angew. Chem., Int. Ed.*, 2012, **51**, 68-89.

11 Y. Zheng, J. Liu, J. Liang, M. Jaroniec, S. Z. Qiao, *Energy Environ. Sci.*, 2012, **5**, 6717.

12 X. Wang, S. Blechert, M. Antonietti, *ACS Catal.*, 2012, **2**, 1596.

13 Z. Lin,X. Wang, *Angew. Chem. Int. Ed.*, 2013, **52**, 1735.

14 Y. Cui, Z. Ding, X. Fu, X. Wang, *Angew. Chem. Int. Ed.*, 2012, **51**, 11814.

15 J. Zhang, M. Zhang, R. Sun, X. Wang, *Angew. Chem. Int. Ed.*, 2012, **51**, 10145.

16 Z. Huang, F. Li, B. Chen, T. Lu, Y. Yuan, G. Yuan, *Appl. Catal., B*, 2013, **136-137**, 269.

17 X. F. Chen, J. S. Zhang, X. Z. Fu, M. Antonietti, X. C. Wang, *J. Am. Chem. Soc.*, 2009, **131**, 11658.

18 F. Goettmann, A. Fischer, M. Antonietti, A. Thomas, *Angew. Chem., Int. Ed.*, 2006, **45**, 4467.

19 F. Goettmann, A. Thomas, M. Antonietti, *Angew. Chem., Int. Ed.*, 2007, **46**, 2717.

20 J. S. Zhang, F. S. Guo, X. C. Wang, *Adv. Funct. Mater.*, 2013, **23**, 3008.

21 M. B. Ansari, H. Jin, S.-E. Park, *Catal. Sci. Technol.*, 2013, **3**, 1261.

22 H. Yan, *Chem. Commun.*, 2012, **48**, 3430.

23 Y. Wang, J. Zhang, X. Wang, M. Antonietti, H. Li, *Angew. Chem., Int. Ed.*, 2010, **49**, 3356.

24 K. Kailasam, J. D. Epping, A. Thomas, S. Losse and H. Junge, *Energy Environ. Sci.*, 2011, **4**, 4668.

25 F. Dong, L. Wu, Y. Sun, M. Fu, Z. Wu, S. C. Lee, *J. Mater. Chem.*, 2011, **21**, 15171.

26 Y. P. Yuan, W. T. Xu, L. S. Yin, S. W. Cao, Y. S. Liao, Y. Q. Tng, C. Xue, *Int. J. Hydrogen Energy*, 2013, **38**, 13159.

27 J. Liu, Y. Zhang, L. Lu, G. Wu, W. Chen, *Chem. Commun.*, 2012, **48**, 8826.

28 M. Shalom, S. Inal, C. Fettkenhauer, D. Neher, M. Antonietti, *J. Am. Chem. Soc.*, 2013, **135**, 7118.

29 Y. S. Jun, J. Park, S. U. Lee, A. Thomas, W. H. Hong, G. D. Stucky, *Angew. Chem., Int. Ed.*, 2013, **52**, 11083.

30 Y.-S. Jun, E. Z. Lee, X. Wang, W. H. Hong, G. D. Stucky, A. Thomas, *Adv. Funct. Mater.*, 2013, **23**, 3661.

31 G. Zhang, J. Zhang, M. Zhang, X. Wang, *J. Mater. Chem.*, 2012, **22**, 8083.

32 F. Dong, Y. Sun, L. Wu, M. Fu, Z. Wu, *Catal. Sci. Technol.*, 2012, **2**, 1332.

33 G. Dong, L. Zhang, *J. Mater. Chem.*, 2012, **22**, 1160.

34 M. Tahir, C. Cao, F. K. Butt, F. Idrees, N. Mahmood, Z. Ali, I. Aslam, M. Tanveer, M. Rizwan, T. Mahmood, *J. Mater. Chem. A*, 2013, **1**, 13949.

35 Y. Cui, J. Huang, X. Fu, X. Wang, *Catal. Sci. Technol.*, 2012, **2**, 1396.

36 J. Zhang, J. Sun, K. Maeda, K. Domen, P. Liu, M. Antonietti, X. Fu, X. Wang, *Energy Environ. Sci.*, 2011, **4**, 675.

37 J. Xu, H. T. Wu, X. Wang, B. Xue, Y. X. Li, Y. Cao, *Phys. Chem. Chem. Phys.*, 2013, **15**, 4510.

38 P. Niu, L. Zhang, G. Liu, H.-M. Cheng, *Adv. Funct. Mater.*, 2012, **22**, 4763.

39 S. Martha, A. Nashim, K. M. Parida, *J. Mater. Chem. A*, 2013, **1**, 7816.

40 X. Zhang, X. Xie, H. Wang, J. Zhang, B. Pan, Y. Xie, *J. Am. Chem. Soc.*, 2013, **135**, 18.

41 A. Du, S. Sanvito, Z. Li, D. Wang, Y. Jiao, T. Liao, Q. Sun, Y. H. Ng, Z. Zhu, R. Amal, S. C. Smith, *J. Am. Chem. Soc.*, 2012, **134**, 4393.

42 X. H. Li, J. S. Chen, X. Wang, J. Sun, M. Antonietti, *J. Am. Chem. Soc.*, 2011, **133**, 8074.

43 Y. J. Zhang, A. Thomas, M. Antonietti, X. C. Wang, *J. Am. Chem. Soc.*, 2009, **131**, 50.

44 S. Zhao, S. Chen, H. Yu, X. Quan, *Sep. Purif. Technol.*, 2012, **99**, 50.

45 E. G. Gillan, Chem. Mater. 2000, **12**, 3906.